Dissociation Dynamics of Oriented DF−HF and HF−DF Complexes: Evidence for Direct and Indirect Dissociation

L. Oudejans and R. E. Miller*

Department of Chemistry, University of North Carolina, Chapel Hill, North Carolina 27599

Received: March 18, 1997; In Final Form: June 10, 1997[⊗]

Photofragment angular distributions have been obtained for HF−DF and DF−HF, resulting from excitation of the H−F stretching vibrations. The hybrid band associated with this vibration in HF−DF allows us access to both the $K_a = 1 \leftarrow 0$ and $K_a = 0 \leftarrow 0$ subbands, while for DF−HF only the $K_a = 0 \leftarrow 0$ transitions are observed. Analysis of these data provides us with detailed information on the final state distribution of the two rotor fragments, including the intermolecular scalar correlations. The dissociation energies (D_0) are determined for both isomers, namely, 1157(2) cm^{-1} and 1082(2) cm^{-1} for HF−DF and DF−HF, respectively. The final state distribution for DF−HF shows that the proton donor molecule gives rise to a highly rotationally excited fragment, while the cofragment arising from the proton acceptor is formed in low-j states, a behavior which is consistent with direct dissociation. For HF−DF the results suggest that dissociation is indirect, in the sense that energy is coupled to states involving the closed DF(v=1) channel prior to dissociation.

I. Introduction

The hydrogen fluoride dimer is somewhat of a prototype system for the study of hydrogen bonding and vibrational dynamics. Prior to the detailed work on the dimer, numerous studies were reported on collisions between HF molecules,[1−4] which also provided important information concerning the relevant interactions. The spectroscopy of the dimer began with work in the microwave,[5−8] which provided insights into both the structure and the tunneling dynamics. More recently the vibrational degrees of freedom have been studied using both near[9−15] and far[16−19] infrared techniques. One of the important advantages of using dimer spectroscopy to study the associated intermolecular forces is that results of this type reflect a well-defined vibrational average over a limited region of the potential. Since the various intermolecular vibrationally excited states sample different portions of the potential surface, it is possible to carry out a systematic exploration in great detail. For a system like HF dimer, which has a highly anisotropic four-dimensional intermolecular surface, this is extremely important since quantities that are averaged over all possible geometries cannot hope to provide information on the detailed shape of the potential. This strength is also the source of the primary weakness of the approach, in that the spectroscopy provides no information in regions where the vibrational wave functions are negligible. Therefore, unless a complete set of vibrational states can be studied, which taken together sample the entire intermolecular coordinate space, there will be regions of the potential that are poorly defined. In fact, even a complete set of bound states is insufficient if the potential is to be determined at energies well above the dissociation limit. Therefore, despite the large number of experimental studies that have been carried out on the HF dimer, there is still considerable need for experiments that probe different parts of the multidimensional surface. This will involve studies of higher lying intermolecular vibrational states of the dimer and its isotopomers, as well as the determination of dissociation energies and state-to-state photodissociation probabilities for the latter.

In parallel with the experimental advances that have occurred in this area, a great deal of theoretical work has been carried out in an effort to better define the six-dimensional potential surface of the dimer.[20−26] In addition, the multidimensional quantum mechanics that connects the intermolecular potential to the spectroscopy is being advanced.[20,27−31] Close coupling calculations have been reported using a four-dimensional intermolecular potential[28,32] in which the intramolecular HF bonds are frozen at their equilibrium distances. Full six-dimensional calculations have also been performed using quantum Monte Carlo (QMC) techniques.[20,27] These calculations give intermolecular bending, stretching and tunneling frequencies, as well as dissociation energies, for the available potential energy surfaces and the different isotopomers of the dimer.[22,26,30,33,34]

As alluded to above, the vibrational predissociation dynamics of this system is also of great interest and can provide us with complementary information on the potential energy surface at energies well above the dissociation limit. Here again, there has been considerable progress in both experiment and theory. It is now well-known that the dissociation dynamics of the dimer is strongly dependent upon which H−F vibration is excited[35,36] and more recently on the number of quanta in each.[13−15] This information comes from the fact that the lifetimes of the vibrationally excited states are strongly dependent upon whether the "free" or "hydrogen bonded" H−F stretch is initially excited.

The question of how the HF fragments are distributed among the open channels was first addressed by Halberstadt et al.[37] using coupled channel methods. On the basis of a pseudo atom−diatom approximation, they found that the proton donor HF monomer fragment is preferentially produced in the highest energetically accessible rotational state. This can be understood on the basis that the proton donor receives a large torque as the molecules separate, while the proton acceptor, approximated by an atom in these calculations, is not torqued since the line of force acts through the associated fluorine atom. Our state-to-state experimental studies[38−41] have confirmed the existence of this high-j − low-j propensity, which is complicated by the fact that the proton acceptor is produced in rotational states other than $j = 0$. This problem has now been addressed theoretically in recent calculations by Zhang and Zhang[34] which include this extra rotational degree of freedom. Overall, the agreement between the calculations and experiment is still only qualita-

[⊗] Abstract published in *Advance ACS Abstracts,* September 15, 1997.

S1089-5639(97)00972-9 CCC: $14.00

tive[34,42] for the available potentials,[20,22,29] illustrating the need for further tests of the latter.

The dissociation energy (D_0) of the HF dimer was first determined to be 1038 (+43, −34) cm^{-1} by Pine and Howard,[43] based on absolute infrared line strengths. This value is consistent with the more recent and accurate value of 1062(±2) cm^{-1} resulting from our photofragment experiments.[39] As we will see below, this method is based on conservation of energy, where the internal and translational energies of the fragments, as well as the energy of the excited state of the parent molecule, are precisely determined. Data of this type provide important constraints on the potential energy surface, and similar data on the isotopomers of the HF dimer would obviously be useful. Indeed, predictions have already been made by Quack and Suhm[20] for the HF−DF and DF−HF complexes. In addition, Farrell et al.[44] have recently reported the observation of symmetry breaking transitions that provide an estimate of the difference in the dissociation energies of the two complexes, namely, $\Delta D_0 = 74.7(5)$ cm^{-1}.

These mixed isotopomers also provide us with a means of keeping track of which fragment came from the proton donor position in the parent dimer and which is associated with the proton acceptor. Thus, detailed final state distributions for these systems could provide us with a means of making a direct link between the high-j−low-j correlation observed in the HF dimer experiments and the proton donor - proton acceptor sites in the complex. We report here the observation of photofragment angular distributions associated with the $K_a = 0 \leftarrow 0$ subband of DF−HF and the $K_a = 0 \leftarrow 0$ and $K_a = 1 \leftarrow 0$ subbands of HF−DF. As indicated above, both complexes have been studied previously by infrared spectroscopy.[44,45] Assignment of the peaks in these angular distributions to final state channels enables us to obtain information on the final state distributions and to determine the absolute dissociation energies for these two complexes. For DF−HF the associated final state distribution is consistent with direct dissociation, where the high-j fragment is the proton donor molecule and the low-j fragment results from the proton acceptor. In contrast, the final state distributions for the HF−DF complex suggest that dissociation is preceded by energy transfer (intermolecular vibrational redistribution (IVR)[46]) or, in other words, is indirect. We propose a mechanism that explains these differences and points out the need for further theoretical work on these systems.

II. Experiment

The apparatus used here to measure the photofragment angular distributions has been discussed in detailed elsewhere.[39,40] The basic idea is to use a continuous wave (cw) infrared (F-center) laser to excite specific states of the parent complex in a small volume on the axis of rotation of the apparatus. A bolometer is positioned so that it can view the photolysis volume from any angle, relative to the molecular beam, as indicated in Figure 1a. Since the lifetimes for dissociation of these complexes are in the nanosecond range, the parent molecules do not move appreciably before they dissociate. As a result, the bolometer can be used to detect the photofragment signal as a function of the recoil angle in the laboratory frame. From the stream velocity of the molecular beam, the maximum recoil angle observed for a particular dissociation channel can be directly related to the translational energy. Assuming that the individual photofragment channels are sufficiently separated in angle so they can be resolved, the internal states can be identified and the intensity associated with each channel can be used to determine the final state probability distribution. The dissociation energy is then determined from conservation of energy.

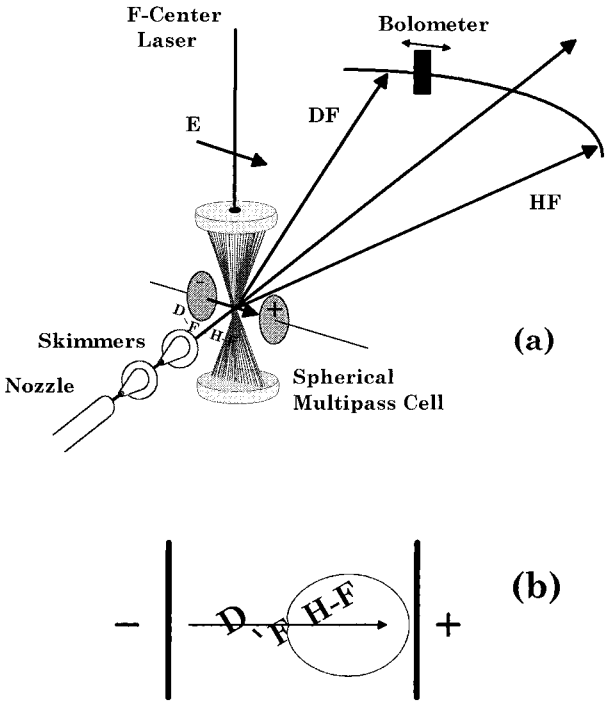

Figure 1. (a) Schematic diagram of the used experimental setup to measure the photofragment angular distributions. The disks on both sides of the molecular beam axis represent the two electrodes that are used to apply a dc electric field to orient the complexes. (b) Square of the $m = 0$ pendular state wave function of DF−*HF, corresponding to the orientation probability distribution. The arrow indicates the direction of the dipole moment of the complex, based on the vector sum of the two separate dipole moments.

As discussed in detail elsewhere,[47] we can also study the dissociation of complexes oriented in a strong dc electric field, based on the "brute force" method.[48,49] This has the advantage that the two fragment molecules recoil in opposite directions in the laboratory frame of reference. This is illustrated in Figure 1b, which shows the orientational probability distribution for the lowest pendular state of the DF−HF complex under the conditions used in the present experiments. At the high electric fields used here (22 kV/cm) the dipole moment of the complex is strongly oriented along the electric field direction such that the DF and HF position themselves on opposite sides of the apparatus. Thus, angular distributions observed to the negative electrode side of the apparatus correspond only to the DF fragment, while the positive electrode angular distribution is that of HF. As we will see in the next section, this ability to separately record the two angular distributions is of considerable advantage in this study.

The mixed isotopomers were formed by expanding a 0.2% HF, 0.5% DF in helium mixture through a 50 μm diameter nozzle from a source pressure of 480 kPa. Under these conditions the stream velocity was measured by Doppler spectroscopy to be $1.701(3) \times 10^5$ cm/s. The transitions of interest in the parent complex were first located by positioning the bolometer at an angle of 5° relative to that of the molecular beam and scanning the F-center laser through the region of interest. Once the transition was located, the laser was locked to a transmission fringe of a 150 MHz confocal etalon located in a separate evacuated chamber. The etalon was then adjusted to make the fringe frequency coincident with the transition of interest. The resulting frequency stability was sufficient to ensure no signal drift over the 30 min required to record an angular distribution, consisting of points separated by 0.25°. By returning periodically to a reference angle, we ensured that the signals did not drift during the measurement due to other

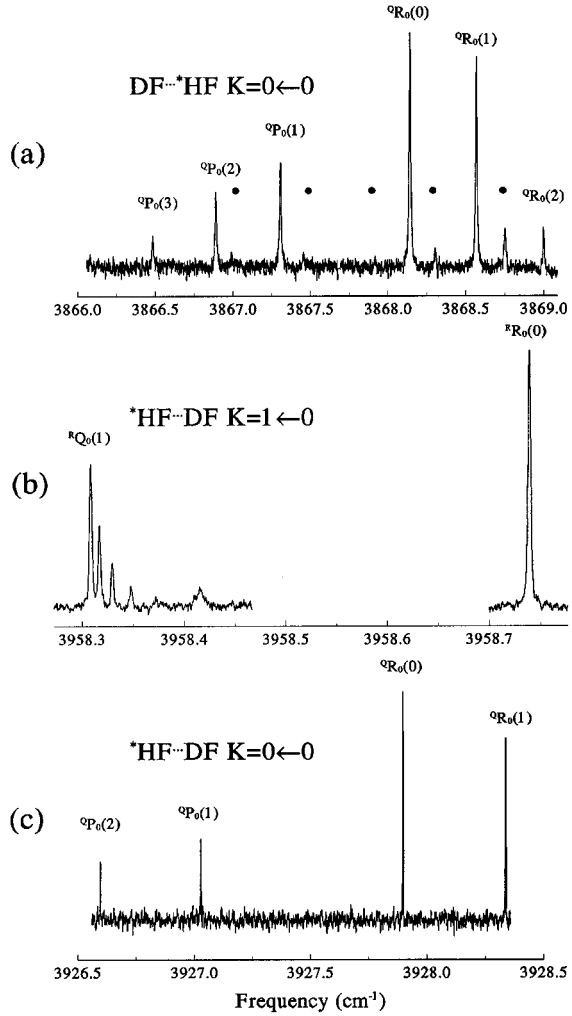

Figure 2. Spectra of the three observed DF−*HF and *HF−DF bands near their vibrational origin. The asterisk refers to vibrational excitation of the specific stretch. The dots in a indicate transitions associated with the n_2 band of the HF dimer, in overlap with this DF−*HF $K_a = 0 \leftarrow 0$ band.

possible sources, such as laser power changes or detector sensitivity changes. It is important to point out that the bolometer only detects a very small flux of photofragments, and thus its sensitivity does not change appreciable over the course of the day. To further minimize possible errors due to drift, the relative intensities for the HF and DF angular distributions were also measured by quickly reversing the polarity of the high-voltage orienting field at various fixed angles.

At the time we began this study the only infrared spectroscopy that had been reported was for the $K_a = 1 \leftarrow 0$ subband of HF−DF.[45] As a result, the other bands reported here were found by searching, using the rotational constants and estimated band origins as a guide. Figure 2 shows three optothermal spectra recorded in the manner discussed above. In this figure the transitions are labeled using symmetric top nomenclature. The homogeneous broadening associated with the DF−*HF complex is clearly visible, while the transitions associated with the two bands of *HF−DF show much smaller line widths. Due to the presence of significant Doppler broadening, resulting from the spherical mulitipass cell, we have not carried out a study of the homogeneous broadening in these spectra, particulary since these widths have been previously reported.[44,45] With use of the convention of Fraser and Pine,[45] the asterisk indicates the subunit that is excited by the laser. In the top panel the dots mark the

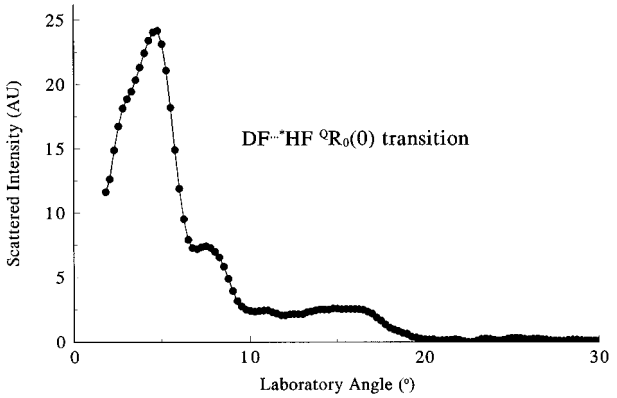

Figure 3. Photofragment angular distribution for the DF−*HF $^{Q}R_0$-(0) transition. The shoulder in the main peak at small angles can be attributed to the DF fragment that scatters to slightly smaller angles than the lighter HF fragment.

HF dimer transitions that also lie in this region of the spectrum. This is expected since HF−HF and DF−HF both have an HF chromophore in a similar "hydrogen bonding" environment. A more complete spectroscopic study of these two isomers has recently been published by Farrell et al.[44] In their study, a "dark" state Q-branch near the vibrational origin of the HF−DF $K_a = 1 \leftarrow 0$ band was observed. They tentatively ascribed this to excitation of the $K_a = 1$ DF−HF dark state, which is nearly resonant with the HF−DF $K_a = 1$ "bright" state. The observed photofragment angular distributions for the $K_a = 1 \leftarrow 0$ subband of HF−DF herein refers to this bright state.

III. Results

A. $K_a = 0 \leftarrow 0$ Subband of the DF−*HF Complex. Photofragment angular distributions were first recorded by tuning the F-center laser into resonance with the $^{Q}R_0(0)$ transition shown in Figure 2a. Figure 3 shows the resulting angular distribution, which has several features associated with different final state fragment channels. Unfortunately, the individual channels are not clearly resolved, due in part to the fact that the bolometer is detecting both HF and DF fragments. Due to their slightly different masses, the corresponding laboratory recoil angles are not the same so that the peaks in the angular distributions are somewhat broader than those observed for the HF dimer. In addition, the rotational constant of the DF is smaller than that of HF and the two fragments are now distinguishable such that the channels labeled $(j_1(\mathrm{DF}),j_2(\mathrm{HF}))$ have a different energy than $(j_2(\mathrm{DF}),j_1(\mathrm{HF}))$. These factors greatly increase the number of fragment channels compared with $(\mathrm{HF})_2$, making them more difficult to resolve.

To improve the resolution and information content of this angular distribution, we carried out pendular state measurements in the manner discussed above. Upon application of a dc electric field (22 kV/cm) to the photolysis region a new band appeared in the spectrum midway between the P and R branches. As discussed in detail previously,[50] these transitions can provide access to the pendular states with the highest degree of orientation. However, due to the significant line broadening associated with the hydrogen bonded H−F vibration in DF−HF, the transitions associated with the various m states were not resolved. Fortunately, at the modest ω values ($\omega = 0.01679 \times \mu\,(D)\,E\,(\mathrm{kV})/B\,(\mathrm{cm}^{-1}) = 5$) used here, the intensities of the $m \neq 0$ transitions, namely, those associated with the less well oriented states, are rather low and do not degrade the orientation of the excited molecules appreciably. It is therefore a good approximation to use the orientational distribution for $m = 0$ shown in Figure 1b.

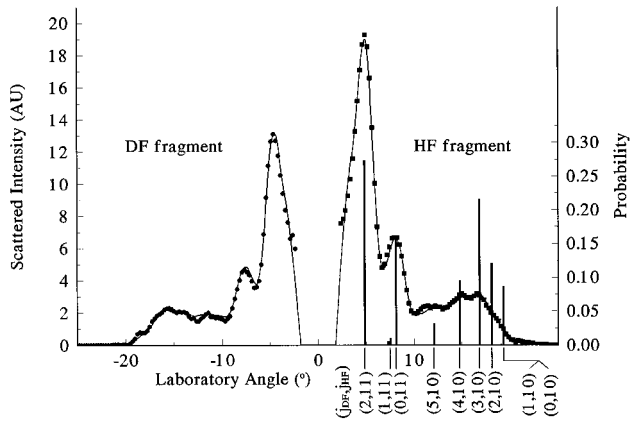

Figure 4. Angular distributions resulting from the photodissociation of oriented DF−*HF. The HF fragments are scattered to positive angles; the DF fragment to negative angles. The solid line through the points is the result of a Monte Carlo fit for both sides simultaneously yielding the probabilities shown by the vertical bars. Only a combined probability is given for the energetically closely spaced (1,10) and (0,10) channel as this probability can be divided arbitrarily over both channels without compromising the quality of the fit.

Figure 4 shows the two angular distributions obtained under the above conditions. The positive and negative angles correspond to the HF and DF fragments, respectively. It is immediately obvious that the peaks in the angular distributions are much better resolved in this experiment, compared with the zero field result shown in Figure 3. Careful inspection of the results shows that the peaks on the DF side appear at slightly smaller angles than the corresponding peaks on the HF side, which is of course expected from the mass difference and conservation of momentum. One thing that is immediately apparent from this figure is that the signal level on the DF side is considerably smaller than that of the HF. To understand these signal levels, we must consider the fact that the bolometer detector measures the energy associated with molecules that "hit and stick". From zero point energy arguments we would argue that the sticking energy of the DF is somewhat higher than that of HF. In addition, the kinetic energy of the DF fragment is higher than that of the HF, since they are both traveling at approximately the same stream velocity, namely, that of the parent DF−HF complex. Note that the stream velocity of these helium seeded beams is large compared with the recoil velocity of the fragments. Finally, since the DF fragment scatters to a somewhat smaller angle than HF, solid angle considerations will also result in larger signals for the former. Despite all of this, we observe that the DF signals are smaller than those of HF, which can only happen if the internal energy content of DF is much less than that of HF. This is the first direct evidence that the high-j (HF fragment)−low-j (DF fragment) correlation[39] applies here. Furthermore, since we now know that the HF is in the proton donor position, we can say conclusively that it is this monomer that gives rise to the high-j fragment.

To make further progress in the analysis of these angular distributions, we must now assign the peaks to specific final state channels. Although the excitation energy is accurately known, given the precision with which we measure the laser frequency, the energy available to the fragments also depends upon the dissociation energy of the parent complex. Fortunately, this is a system for which the theoretical work is quite advanced and we can make use of the calculations of Quack and Suhm as a starting point.[20] These calculations should be quite reliable, particularly for those based on a semiempirical potential that was adjusted to reproduce our previously determined value for the dissociation energy of the HF dimer,[20] since the only

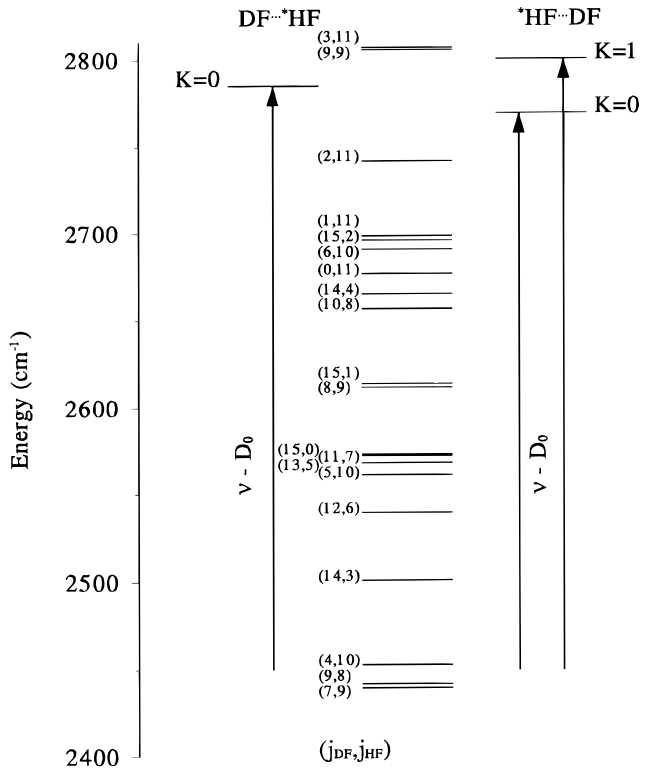

Figure 5. Photofragment energy level diagram for the photodissociation of DF−*HF and *HF−DF. The arrows show the amount of energy available to the fragments. The $K_a = 0$ and $K_a = 1$ labels indicate states of the complex; the rotational quantum numbers refer to the DF and HF fragment, respectively.

difference was in the zero point energy. The most recent calculations[51] suggest a value of 1078 cm^{-1} for the DF−HF complex, while those of Zhang et al.[30] give 1078.5 cm^{-1}. These values are in excellent agreement with our preliminary result for this system (1080 cm^{-1}),[42] which was based solely on the zero field angular distribution discussed above. In the present study we refine this value to 1082(2) cm^{-1} using the pendular state angular distributions. This is done by adjusting the dissociation energy until the kinetic energy releases for the various channels are such that the corresponding peaks appear at the proper angle. In particular, the position of the first peak in the angular distributions shown in Figure 4 is very sensitive to the dissociation energy.

Figure 5 shows an energy level diagram based upon a dissociation energy of 1082 cm^{-1}. The fragment energy levels are shown in the center of the diagram, corresponding to production of correlated fragments (j_{DF},j_{HF}). The energy level to the left marks the position of $K_a = 0$ of the DF−*HF complex, shifted by the dissociation energy of the complex so that it corresponds to the total available energy of the system. It is a fortunate coincidence that this state lies between two widely separated fragment states, since to bring another channel to the correct recoil energy, the dissociation energy would have to be changed by a large amount (approximately 40 cm^{-1}), which is well outside the anticipated error. Thus, the assignment of the (2,11) channel as the first open channel is unique. As expected from the magnitudes of the DF versus HF signals, this channel corresponds to a low j DF fragment and an HF in high j. With a dissociation energy of 1082 cm^{-1}, the translational energy release for this channel is 44 cm^{-1}. Making use of the stream velocity determined above, this corresponds to maxima in the photofragment intensities for the HF and DF fragments of 4.85 and 4.55°, respectively, in good agreement with experiment.

TABLE 1: State-to-State Probabilities and Recoil Energies for the Open Channels in the Photodissociation of DF−HF and HF−DF

	DF−*HF ($K = 0 \leftarrow 0$)		*HF−DF ($K = 1 \leftarrow 0$)			*HF−DF ($K = 0 \leftarrow 0$)		
fragment channel ($j_{DF}j_{HF}$)[a]	recoil energy (cm^{-1})	probability	I[b]	recoil energy (cm^{-1})	probability	II[b]	recoil energy (cm^{-1})	probability
(2,11)	43.6	0.274	a	59.4	0.027	a	28.3	0.004
(1,11)	87.0	0.006	b	102.8	0.228	b	71.7	0.005
(6,10)	94.6	0.010	c	110.5	0.042			
(0,11)	108.7	0.158	d	124.5	0.035	c	93.5	0.005
(5,10)	224.5	0.032	e	240.3	0.041	d	209.2	0.056
(4,10)	332.8	0.095	f	348.6	0.134	e	317.5	0.166
(3,10)	419.5	0.216	g	435.3	0.203	f	404.3	0.038
(10,7)						g	438.2	0.041
(2,10)	484.6	0.121				h	469.4	0.095
(11,6)			h	518.4	0.100	i	487.3	0.084
(1,10),	528.0	0.087						
(0,10)	549.8							
(8,8)			i	553.3	0.017			
(13,3)						j	566.8	0.030
(5,9)			j	643.0	0.029	k	612.0	0.187
(9,7)			k	684.1	0.023			
(12,4)			l	711.2	0.010	l	680.1	0.080
(4,9)				751.3				
(10,6),				754.2	0.038	m	723.1	0.078
(11,5)				763.3				
(13,1),				803.2				
(3,9),			n	838.1	0.063			
(13,0)				844.3				
(8,7)						n	846.9	0.087
(7,7)						o	1019.4	0.042

[a] Channels that are grouped together cannot be distinguished, based purely on the angular distribution. [b] The alphabetic indices refer to the vertical bars in Figure 7 (I) and Figure 8 (II).

Having assigned the first peak in the angular distribution, we can now calculate the energy difference between the (2,11) channel and the one that is responsible for the second peak near 8°. The situation is a little more complicated in this case since there are a group of closely spaced levels in this region, corresponding to total internal energy in the fragments between 2650 and 2700 cm^{-1}. It is interesting to note, however, that most of these levels corresponding to final states in which the DF fragment is in high j and the HF in low j, such as (15,2), (14,4), and (10,8). These can all be eliminated as the primary channels since they would result in the signals on the DF side of the angular distribution being larger than on the HF side, which is clearly not the case. In fact, the only channel that is consistent with the microcalorimetry and lies at the correct energy for the peak at 8° is (0,11). Although the (1,11) channel must be between (2,11) and (0,11), there is no obvious peak in the angular distributions. As we will see, dissociation into (1,11) is not favored, for reasons that are not at all obvious.

From the combination of bolometer microcalorimetry (comparing the energy content of the two fragments as determined by the relative bolometer signals) and the energetics implied by the angular distributions, we have shown that the small angle portion of these distributions is entirely due to channels corresponding to $j_{HF} = 11$. The fact that the ratios of the sum of the DF to HF internal plus surface sticking energies are approximately the same for the (2,11), (1,11), and (0,11) channels (namely, 0.351, 0.341, and 0.335, respectively) explains why the ratios of the intensities of the first and second peaks are the same on the HF and DF sides of the angular distribution. Given that the ratio of the HF to DF signals is approximately constant for all corresponding angles, we conclude that the additional structure at larger angles must be due to channels with similar ratios to those given above. The most reasonable assignment is to the next lowest HF fragment state, namely, the channels with $j_{HF} = 10$. As the vertical bars (positioned at the angle of maximum intensity for each channel) in Figure 4 illustrate, these $j_{HF} = 10$ channels account for all of the remaining intensity in this angular distribution. Our conclusion is that only channels with $j_{HF} = 10$ and 11 contribute appreciably to the dissociation of the DF−*HF complex. We should point out here that small (<2%) contributions from the other channels would be difficult to detect using this approach, and in all of the subsequent analysis we ignore them.

Now that we have determined the primary contributing channels, the next step is to fit the angular distributions to determine the state-to-state photodissociation probabilities. A Monte Carlo approach was used to calculate the shape of the individual channels in the angular distributions, as discussed in detail elsewhere.[38,40] The data were then fit by adjusting the individual final state probabilities. This was done for a range of dissociation energies near 1080 cm^{-1}, which showed that the best fit resulted from a dissociation energy of 1082 cm^{-1}, as indicated by the solid line through the data in Figure 4. The heights of the vertical bars in Figure 4 give the probabilities for the various channels. It is interesting to note that the probabilities for the (2,11) and (3,10) channels are rather similar even though the intensities of the corresponding peaks are very different, the latter being much weaker. This can be understood by considering that the higher kinetic energy associated with the (3,10) channel results in scattering into a larger solid angle compared with (2,11). As a result, the bolometer collection efficiency is higher for the (2,11) channel than for (3,10). Table 1 summarizes the probabilities obtained from this fitting procedure.

Since there are only three channels associated with the $j_{HF} = 11$ channel, it is difficult to say much about trends. It is interesting, however, to notice that the (1,11) channel has an anomalously low probability, compared with those of (0,11) and (2,11). Unfortunately, without the aid of theoretical calculations, we can offer no significant insight into this phenomena, other

than to say that such large oscillations in the probabilities seem characteristic of some form of interference effect. The trend for the $j_{HF} = 10$ channels is more obvious. Here the probability increases with increasing j_{DF}, in agreement with statistical arguments, up to (3,10) and then decreases for higher j_{DF}. We propose that this reduced probability for higher j_{DF} states is a dynamical effect, namely, that for the higher j_{DF} channels there is simply insufficient torque applied to the DF fragment to appreciably populate these states. We will have more to say regarding the comparisons between the experimental results and statistical PST later.

It is important to point out that we searched extensively for other possible assignments of the angular distribution shown in Figure 4. Fortunately, no other combination of states is consistent with both the data and the theoretical estimate of the dissociation energy.[51] Indeed, one would have to change the dissociation energy by 60 cm^{-1} in order to obtain another fit to the data based on the first peak being due to ($j_{DF} = 3$, $j_{HF} = 11$) instead of ($j_{DF} = 2$, $j_{HF} = 11$). This is far outside the acceptable range, making the assignment given here unique.

The best fit shown in Figure 4 was obtained with a center-of-mass photofragment angular distribution slightly broader than the δ function implied by an impulsive dissociation process. It is difficult to quote an anisotropy parameter (β)[40] for this case since the pendular state angular distributions are sensitive to higher moments of the recoil distributions. Nevertheless, we estimate that the center-of-mass distribution is approximately as broad as a $\cos^4\theta$ distribution. Some of this may be due to the fact that the pendular spectra were broad, and the laser did not excite a pure $m = 0$ state. Finally, we used the probabilities obtained from the pendular state results to calculate the zero field angular distribution shown in Figure 3, and the agreement was excellent. This shows that the electric field does not significantly change the dissociation probabilities.

B. $K_a = 1 \leftarrow 0$ Subband of *HF−DF. Having obtained an accurate value for the dissociation energy of the DF−HF complex in the previous section, we can now determine the value for the HF−DF isomer by making use of the dissociation energy difference (74.7 cm^{-1}) obtained spectroscopically by Farrell et al.,[44] yielding 1157(2) cm^{-1}. This is in good agreement but still outside our error bars with the theoretical calculation of Klopper et al.[51] which gave 1154 cm^{-1}, based on their latest potential energy surface. For HF−DF this approach provides a better estimate of the dissociation energy than starting over again with the procedure discussed above, for reasons that will be discussed below.

We begin our discussion of the *HF−DF complex with the $K_a = 1 \leftarrow 0$ subband. The angular distribution was first recorded under zero electric field conditions with the laser polarization direction both parallel and perpendicular to the molecular beam.[40] The results obtained in this way for the $^RR_0$(0) transition (see Figure 2b) are shown in Figure 6a,b, respectively. In the former case the laser polarization is such that the excited molecules are preferentially aligned perpendicular to the molecular beam, yielding fragments that tend to recoil to the maximum possible laboratory angle. For perpendicular polarization, the alignment is along the beam direction, resulting in large fragment intensities near zero degrees. Note that since we are pumping individual rovibrational eigenstates, there is no rotational dephasing even though the predissociation lifetimes are long. The energy diagram in Figure 5 shows that the available energy in the $K_a = 1$ state of the HF−DF complex is similar to that of the $K_a = 0$ level of DF−HF. Although the dissociation energy of HF−DF is greater than that of DF−HF (this can be understood from zero point energy considerations),

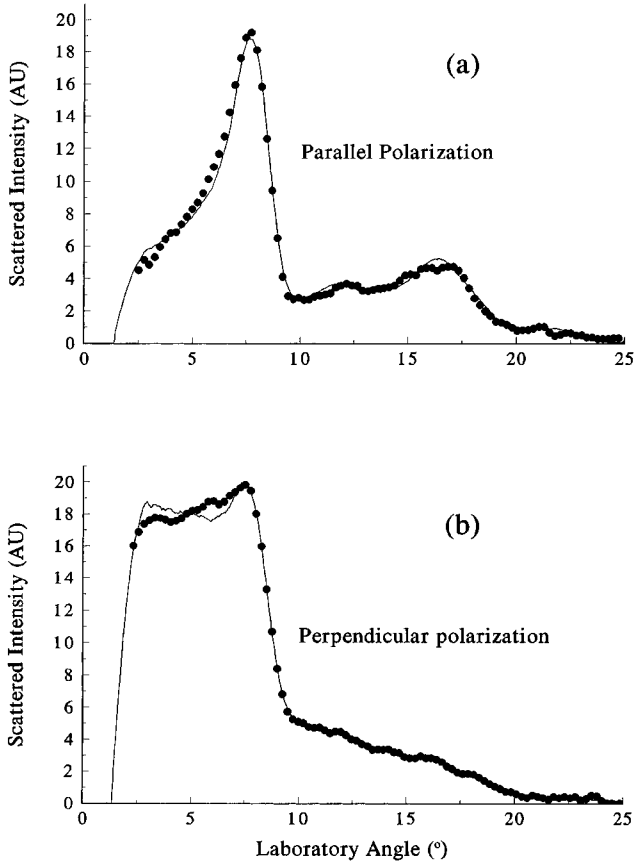

Figure 6. Photofragment angular distributions obtained for the $^RR_0$(0) transition of *HF−DF for two laser polarizations. The solid line in a is a fit to the parallel polarization data for a dissociation energy value of $D_0 = 1157$ cm^{-1}. The solid line in b was calculated with no adjustable parameters from the probabilities obtained from fitting a.

this difference is compensated for by the fact that we are exciting a "free" H−F stretch in *HF−DF, which has a smaller red shift with respect to the HF monomer vibrational band origin. When combined with the fact that we are also exciting one quantum of K_a rotation, the excitation energy is larger than for DF−HF by an amount that is approximately the same as the dissociation energy difference. This gives us the opportunity of looking at the dissociation of these two isotopomers from essentially the same energy, which means the same set of photofragment states, ideal for determining how the dynamical propensities differ for the two systems.

The first thing that is evident in the angular distribution shown in Figure 6a is the fact that the first peak is shifted to larger angles, when compared with those of DF−HF. Since the available energies are approximately the same, we must conclude that the (2,11) channel is no longer dominant. Assigning the first peak in Figure 6 to a specific final state channel is complicated by the fact that three states lie very close together in energy, namely, (1,11), (15,2), and (6,10), and therefore any one or combination of these three states could explain the first peak in Figure 6a. In fact, one obtains a slightly different dissociation energy, depending upon which is chosen as the primary channel.

It is tempting to suggest that the reason the (2,11) channel is not observed in this angular distribution is that the system again has a strong propensity, in this case for states with large j_{DF} and small j_{HF}. On the basis of a direct dissociation mechanism we would indeed expect this reversal, due to the change in the proton donor−proton acceptor roles for the HF and DF subunits. If such a propensity indeed exists, the obvious choice from the (1,11), (15,2), and (6,10) channels to explain the first peak in

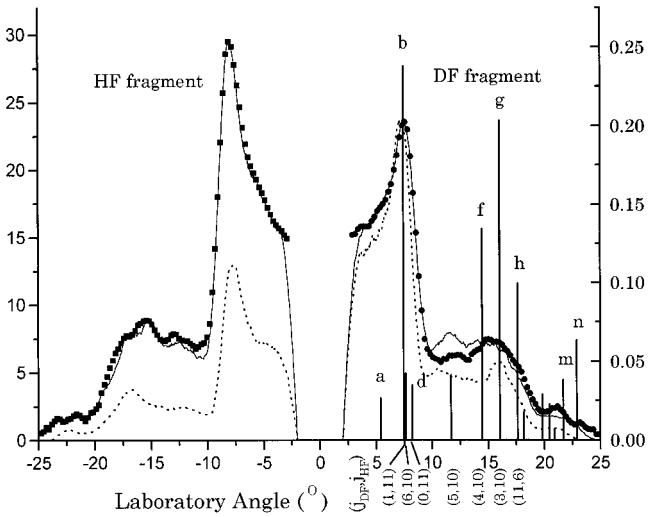

Figure 7. Photofragment angular distributions resulting from the photodissociation of oriented *HF−DF, $K_a = 1 \leftarrow 0$. The solid line through the experimental data points is a simultaneous fit to the two angular distributions. The vertical solid bars represent the resulting probabilities. The alphabetic index is provided to avoid congestion and corresponds to the (j_{DF},j_{HF}) channels tabulated in Table 1. The dotted lines represents the best fit to the DF side where only the high-j_{DF}−low-j_{HF} channels are included. The resulting probabilities were then used to calculate the HF distribution, clearly showing that there is no propensity for the high-j_{DF}−low-j_{HF} states.

the angular distribution would be (15,2). Continuing with this line of argumentation, we can indeed accurately fit the entire angular distribution by including only the high-j_{DF}−low-j_{HF} channels, as indicated by the solid line shown in Figure 6a. It is interesting to note that probabilities determined from fitting the parallel polarization angular distribution (Figure 6a) were used to calculate the perpendicular polarization data (Figure 6b), shown as the solid lines in Figure 6. To obtain this good agreement between the two angular distributions, and indeed to reproduce the data in Figure 6a, the β parameter had to be reduced from the axial recoil value (namely, -1 for a $^{R}R_0(0)$ transition) to be -0.5.

The above method for assigning the angular distributions in Figure 6 is clearly not the most desirable since it requires that we make assumptions about which of the available states are populated. One approach we have used to overcome this limitation is involves a second laser to probe the internal states of the fragments.[52] Unfortunately, this method was not applicable in this case due to insufficient signal levels on these mixed dimers. The other approach is the one discussed above for DF−HF, namely, orienting the parent molecules and using microcalorimetry to determine the relative energy content of the two fragments. Experiments of this type are somewhat more complicated for the present case where we are exciting the complex to $K_a = 1$. As a result, we cannot use the simple linear molecular Hamiltonian that is representative of the $K_a = 0 \leftarrow 0$ band. A full discussion of the pendular state spectroscopy of an asymmetric rotor will be given elsewhere. It is sufficient for the present purposes to note that we have identified transitions in this perpendicular band that populate oriented states in $K_a = 1$ so that we can obtain results analogous to those reported above for DF−HF. It is interesting to note that since the sign of the dipole moment is reversed, compared with DF−*HF, the HF and DF angular distributions are reversed compared with the results in Figure 4.

Figure 7 shows a set of oriented complex angular distributions obtained by tuning the laser to the pendular features identified in the spectrum. Careful inspection again shows that

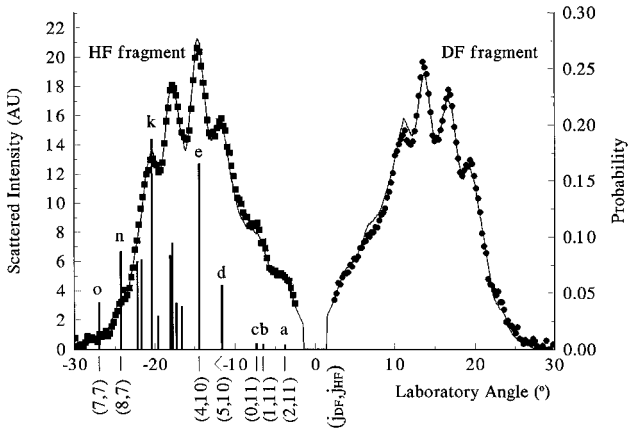

Figure 8. Photofragment angular distributions for oriented *HF−DF, $K_a = 0 \leftarrow 0$. The solid line through the experimental points corresponds to a simultaneous fit to both angular distributions with the dissociation energy fixed to the value as determined from the $K_a = 1 \leftarrow 0$ band. The solid vertical bars indicate the resulting probabilities for each channel. The alphabetic index is provided to avoid congestion and corresponds to the (j_{DF},j_{HF}) channels tabulated in Table 1.

the peaks on the side corresponding to the DF fragment occur at slightly smaller angles than the corresponding peaks on the HF side. The fragment assignments given in the figure are also consistent with the direction of the dipole moment in this complex. What is immediately obvious and surprising is the fact that the signals on the HF side are larger than those on the DF side. This is exactly the same behavior observed above for the other isomer and inconsistent with the argument given above based on the proton donor−proton acceptor roles of the DF and HF subunits. Indeed, the dotted lines shown in the figure result from calculations based upon the fit shown in Figure 6, which includes only the high-j_{DF}−low-j_{HF} channels. As one might expect, this gives angular distributions that are stronger on the DF side, relative to HF. The obvious implication is that the simple propensity rule does not apply in this case. We will postpone further discussion of this interesting aspect of the study until we have completed the reevaluation of the data.

In light of this new information we must clearly rethink the assignment given above for the HF−DF $^{R}R_0(0)$ angular distribution. Indeed, of the triplet of channels that are capable of explaining the first peak in the angular distributions, the (15,2) is clearly not the major contributor, leaving the (1,11) and (6,-10) channels. In fitting these pendular angular distributions, we included all three channels, even though the fitted (15,2) probability was extremely low. We fit the two pendular angular distributions simultaneously to obtain the solid lines shown in Figure 7. The vertical bars give an indication of the relative importance of the various channels, although in this case the probabilities are somewhat correlated and in some cases (mainly at larger angles) probability can be exchanged between adjacent channels without seriously compromising the fit. With these limitations in mind, we give the probabilities in Table 1. Note that the primary channel responsible for the first peak is (1,11). It is important to note that the discussion of the β parameter given above, determined from fitting the parallel and perpendicular polarization results at zero electric field, is not affected by the reassignment of the channels since the shape of the peaks depends only on the recoil energy and not on the identity of the final states.

C. $K_a = 0 \leftarrow 0$ Subband of *HF−DF. Since the H−F stretch in HF−DF gives rise to a hybrid band, the $K_a = 0 \leftarrow 0$ subband also has significant intensity[44] (see Figure 1c). Figure 8 shows the angular distributions obtained for this system, corresponding to excitation of the $m = 0$ state. Consistent with

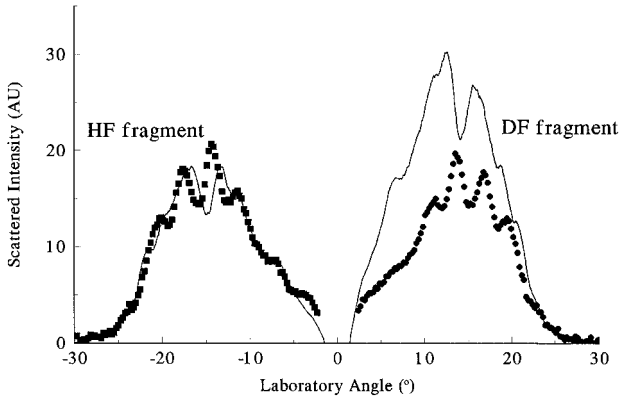

Figure 9. Comparison between the experimental angular distributions for oriented *HF−DF, $K_a = 0 \leftarrow 0$, and the best fit to the HF side where only the low-j_{DF}−high-j_{HF} channels are included. The resulting probabilities were then used to calculate the DF distribution, clearly showing that there is no propensity for the low-j_{DF}−high-j_{HF} states.

the polarity of the parent complex, we again observe the HF and DF fragments on the appropriate sides, as confirmed by the positions of the peaks (larger angles for HF than DF). Once again, we find that the microcalorimetry does not support the picture that the proton donor molecule (in this case DF) carries away most of the excess energy in the form of rotation. Indeed, the intensity is slightly larger on the HF side. Even more interesting is the fact that the angular distributions have much more extensive structure and extend to much larger angles than in the previous cases, indicative of a larger average kinetic energy release. As indicated in the energy level diagram shown in Figure 5, the available energy is rather similar to the other cases and the open channels are the same. There is clearly a dramatic change in the dynamical behavior of this system in going from $K_a = 1$ to $K_a = 0$. Such a large difference in the final state distribution for such a small change in energy is surprising, and we will say more concerning this somewhat later.

Figure 9 shows a fit to the HF side with only a restricted number of open channels, i.e. only the high-j_{DF}−low-j_{HF} states. It is immediately clear that the experimental angular distribution for the HF fragment cannot be reproduced by these channels and that the intensity on the DF side is strongly overestimated owing to the correspondingly high internal energy. We must again conclude that, despite its proton acceptor location, the HF fragment carries a significant amount of rotational energy.

The solid line through the data in Figure 8 is a fit to the data including all 56 final state channels using the dissociation energy for this isomer determined above. Close inspection of the HF side at small angles reveals two features (at 3.5 and 7.5°) which are not present in the DF angular distribution. These coincide with and are assigned to the $j_{HF} = 11$ states (0,11), (1,11), and (2,11). Not only are the positions of these channels consistent with the features in the HF angular distribution, but the concentration of the available energy in the HF fragment, combined with their low probability, explains why they are not observed on the DF side. Although the number of features in the angular distributions are insufficient to make a unique assignment based purely on the peak positions, the situation is made considerably better by the microcalorimetry. In fact, by fitting to both distributions simultaneously, having to ensure that the relative intensities as well as the peak positions are reproduced, the final state distributions become much more unique, to the point where many of the channels are clearly identified. Therefore, although the probabilities given in Figure 8 and tabulated in Table 1 need to be viewed with some caution, they certainly give the correct qualitative picture for the final state distribution for this case. Indeed, the most important

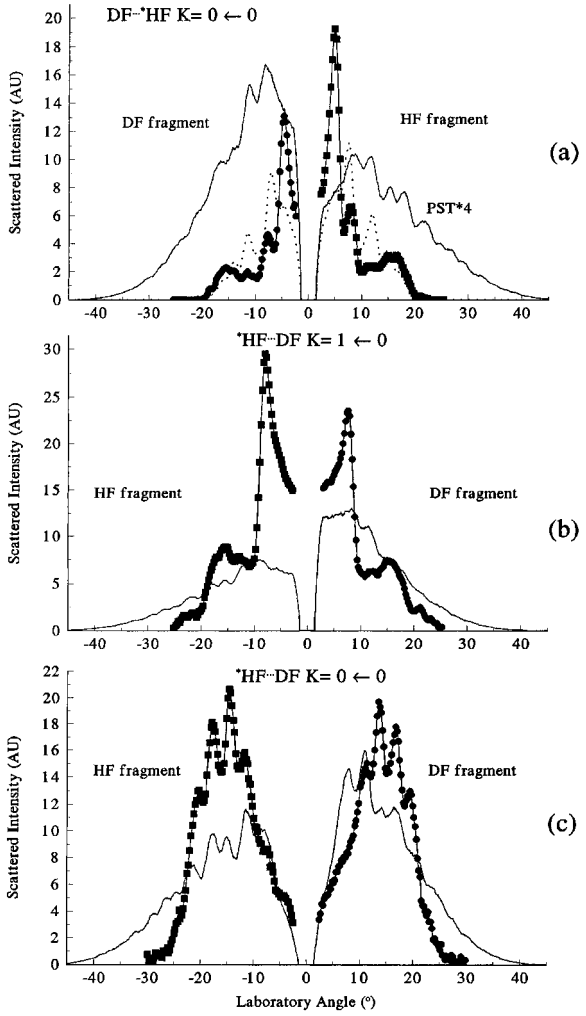

Figure 10. Comparison between the PST calculations and the experimental angular distributions for DF−*HF and *HF−DF. The solid curves represent full statistical calculations; the dashed curve in a represents a restricted PST calculation in which only the $j_{HF} = 11$ and 10 are included.

conclusion is that the high-j−low-j type sorting is not observed in this case. It is also interesting to note that the average kinetic energy release obtained from these probabilities is 519 cm^{-1}, considerably larger than the 360 cm^{-1} for the $K_a = 1$ state of *HF−DF and 268 cm^{-1} for the $K_a = 0$ state of DF−*HF.

IV. Discussion

To summarize the results of the previous section, we note that for the DF−HF complex a high-j_{HF}−low-j_{DF} propensity is observed, consistent with the proton donor−proton acceptor equilibrium structure from which dissociation occurs in a direct fashion. Since this is the first of the mixed isotope dimers we analyzed, it seemed as if all was consistent with our previous ideas, based upon HF−HF.[39]

In a number of previous studies[39,47,54,55] we have found it useful to compare the results of our experiments with those of phase space theory (PST).[56] In general, we have found that the results of a fully unconstrained (except for energy and angular momentum) PST calculation are in poor agreement with experiment. This is not particularly surprising given that the dynamics of weakly bound complexes are known to be highly nonstatistical. However, in previous studies we have found that by imposing some intuitive dynamical constraints, a restricted form of PST often did quite well.[55] As shown in Figure 10a, the unrestricted PST calculation again gives very poor agreement

with experiment. First it tends to over estimate the importance of the channels where the two rotational quantum numbers are nearly the same, since this maximizes $(2j_{DF} + 1)(2j_{HF} + 1)$. Second, it is not selective enough, tending to grossly overestimate the average kinetic energy release. Even if we constrain the j_{HF} quantum number to the experimentally observed ones, namely, 10 and 11, the agreement with experiment is still poor as indicated by the dotted curve in Figure 10a. The difference is related to the apparent dynamical constraint mentioned above, namely that for a given HF fragment state the probabilities only increase with j_{DF} for small values of the latter. At larger j_{DF} the experimental probabilities decrease, which we propose is due to the inability of the system to apply significant torque to the DF (proton acceptor) fragment. Therefore, as with the HF−HF system,[39] all degrees of freedom of the DF−HF system appear to be highly nonstatistical and yet rather straightforward to explain based upon the direct dissociation mechanism.

As noted above, the situation is very different for the HF−DF complex. In both the $K_a = 0$ and $K_a = 1$ states we observe final state distributions that are inconsistent with our proton donor−proton acceptor picture. In this case the proton acceptor molecule (HF) somehow does receive a large torque, as evidenced by the high-j_{HF} states observed. In considering explanations for this difference, it is important to point out that this system may have a bias toward exciting the HF rotor, given that the associated rotational constant is much larger than for DF. As a result, excess energy can be more efficiently accommodated by the HF without the necessity of populating very high j states. For example, it takes 15 quanta of DF rotation to accommodate approximately the same energy as 11 quanta of HF rotation. Therefore, if a mechanism exists for funneling energy into the HF rotational degree of freedom, we might expect that the system would make use of it. Remember that large Δj transitions require high- order terms in the anisotropy of the potential surface, so that dissociation into states with large Δj is expected to be slow. For HF to be excited, however, the system must configure itself so that it can receive a large torque during the dissociation process. The implication is that the dissociation is not direct but rather proceeds indirectly through states that have a vibrationally averaged structure very different from that of the equilibrium geometry. For example, if the excited state is coupled to states in which the monomer units are not as angularly constrained as they are in the ground state (large bending excitation, for example), we might expect that the simple high-j−low-j propensity would no longer hold.

Before discussing possible candidates for such an indirect (IVR type) dissociation process, we note that this idea is further supported by the fact that we observe such a large difference between the final state distributions for the $K_a = 0$ and $K_a = 1$ states of this system. Since the energy difference is very small and the available channels are the same for these two states, this observation is quite surprising. Indeed, it is generally observed that small changes in the rotational energy content of the parent molecule have little effect on vibrational predissociation dynamics. We therefore conclude that the effect we are looking at is not simply a result of the change in the angular momentum or energy of the system. A more likely explanation is that there is weak coupling to states with very different character. Such weak couplings (perturbations) tend to change dramatically with rotational excitation since they often depend critically (at the level of fractions of a wavenumber) on the energy spacing between the unperturbed bright and dark states.[46]

In this context, it is interesting to point out that Farrell et al.[44] have indeed observed weak perturbations in the *HF−DF spectroscopy, which they attribute to the asymptotically closed DF(υ=1) + HF(υ=0) channels, as shown in Figure 11. The transitions for which they observe these perturbations are associated with relatively high j states of the $K_a = 1$ manifold. Although the lower j states observed here are certainly perturbed to a lesser extent, we must remember that vibrational predissociation is a rare event so that even very weak couplings can have a major effect. Although there is no evidence from the spectroscopy that the $K_a = 0$ state is perturbed,[44] weak anharmonic coupling could go unnoticed and still have a major influence on the dynamics. Once again, the large difference between the final state distributions for $K_a = 0$ and $K_a = 1$ strongly support this perturbation picture.

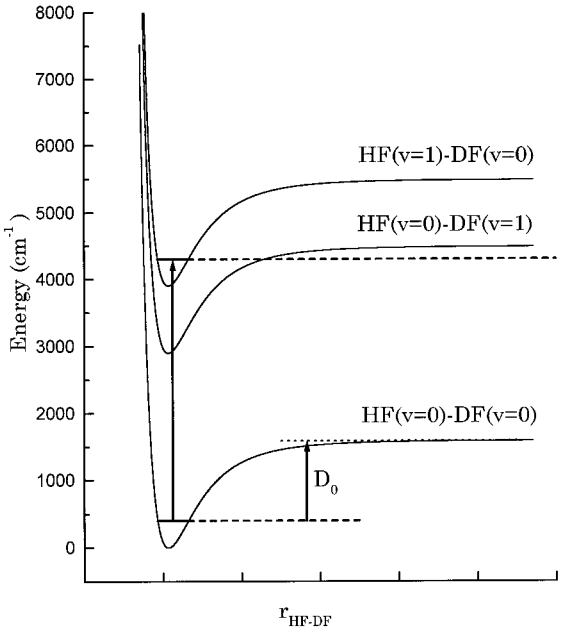

Figure 11. Energy diagram showing the potential energy curves relevant to the photodissociation dynamics of the *HF−DF complex. The vertical arrow indicates the vibrational excitation of the HF subunit in the complex. We propose that HF−DF dissociation proceeds via coupling between the initially excited HF(υ=1)−DF(υ=0) state and the asymptotically closed HF(υ=0)−DF(υ=1) channels.

It is evident from Figure 11, which is drawn to scale, that the initially excited states of the complex are imbedded in a manifold of states associated with the asymptotically closed DF(υ=1) channel. The important dark states obviously correspond to large intermolecular excitation on the DF(υ=1) potential, even well above the isomerization barrier (360 cm^{-1} for the HF dimer[51]). As a result, these states could provide the delocalization needed to eliminate the proton aceptor-proton donor character. Depending upon the exact nature of the dark state in question, the final state distributions could then be quite different from one state to another, accounting for the large difference observed experimentally for the $K_a = 0$ and $K_a = 1$.

Relevant to this discussion is the previous dynamical work we have reported on the HF dimer, corresponding to excitation of the intermolecular stretching and bending vibrational modes in combination with the H−F stretch.[41] Upon excitation of the intermolecular F−F stretching combination band the product state distribution, although somewhat different from those associated with the fundamental, owing to the opening of several channels, still shows the high-j−low-j correlation. However, there is an increase in the average kinetic energy release, equal to the additional energy associated with the F−F stretching mode. Upon excitation of the intermolecular geared bending combination band the kinetic energy release does not change compared with the fundamental, while the high-j−low-j correlation in the photofragments is somewhat less prominent. This

is attributed to the fact that, upon excitation of this bending mode, the proton donor and acceptor roles become somewhat less distinguishable due to the much larger bending amplitude, thus making the two molecules more dynamically similar. These results show that changes in the intermolecular vibrational wavefunctions of these complexes can indeed alter the final state distributions.

Parts b and c of Figure 10 show comparisons between the experimental results for both bands of HF−DF and those from PST. Once again, the $K_a = 1 \leftarrow 0$ angular distributions are highly nonstatistical. The situation is rather different for the $K_a = 0 \leftarrow 0$ angular distributions, where PST is at least qualitatively correct. Indeed, as noted above, the average kinetic energy observed experimentally in this case is considerably larger due to the population of many more final states. A more statistical distribution might indeed be expected if the parent complex, prior to dissociation, has the opportunity to sample a much wider range of its configuration space due to coupling to the DF(v=1) surface.

An important question to address is why the DF−HF and HF−DF systems behave so differently, the first conforming to our high-j−low-j picture and the second not. As pointed out previously, one reason is simply that the HF fragment is always the preferred depository of energy, due to its large rotational constant. Therefore, all else being equal, we might expect this fragment to preferentially carry away the excess energy. Nevertheless, we submit that for dissociation from the equilibrium geometry this bias would not be satisfied for HF−DF since the HF fragment cannot be torqued appreciably. We therefore need a mechanism for moving the system away from this asymmetric geometry. It is interesting to note that the lifetime of the HF−DF complex is much longer (see Figure 2) (10−100 times longer[44]) than that of DF−HF. As a result, the HF−DF complex has much more time to sample the dark states, which is the same as saying that very weak couplings can have a significant influence on the dynamics. In fact, part of the reason for the large difference in lifetimes, in addition to the obvious difference between the free and hydrogen bonded stretches, may be that the system prefers to put energy into the HF but can only do so through the indirect process involving the DF(v=1) surface. Clearly these ideas should be explored and tested further by carrying out multidimensional dynamics calculations, which are feasible for these systems.[31,34,57]

V. Summary

We have reported photofragment angular distributions for a number of vibrational bands associated with the DF−*HF and *HF−DF isotopomers. These distributions show sufficient structure to allow us to make assignments of the final state distributions. Knowing the excitation energy, the recoil energy of a particular fragment channel, and the corresponding internal energy of that state, we have determined the dissociation energy of the DF−HF complex to be 1082(2) cm^{-1}, which compares favorably with that predicted by theory, namely, 1078 cm^{-1}.[30,51] We then make use of the spectroscopic dissociation energy difference obtained by Farrell et al.[44] to determine the dissociation energy of the second isomer, HF−DF, yielding 1157(2) cm^{-1}, which is again in good agreement with the most recent calculations of Klopper et al.[51] (1154 cm^{-1}).

The final state distributions determined for DF−HF clearly confirm the high-j−low-j correlation reported previously for the case of HF dimer. The present results show that the high-j fragment correlates with the proton donor in the complex, while the low-j fragment results from the proton acceptor. To date, there have been no theoretical calculations of the final state distributions for the mixed isotopomers of HF dimer, although the theoretical framework for doing such now exists.[51] As a result, the only comparison we can make with theory is with a simple phase space calculation. This comparison reveals an additional propensity of the system for production of fragments in states with relatively low recoil energies.

For HF−DF we observe final state distributions that do not conform to the low-j_{HF}−high-j_{DF} ideas. We propose that this is due to coupling to the asymptotically closed DF(v=1) channels, resulting in angular delocalization of the parent complex which allows the system to populate high-j states of the HF subunit. We propose that the large difference between the final state distribution for $K_a = 0$ and K_a=1 of HF−DF results from the fact that these two bright states couple to different dark or "doorway" states[46] with very different intermolecular vibrational character. The experimental results show conclusively the breakdown of the high-j−low-j correlation for *HF−DF. Nevertheless, the high density of fragment states leads to some ambiguities in the detailed final state distribution, particulary for the $K_a = 0 \leftarrow 0$ subband. Future experiments could overcome this difficulty by state selectively probing the fragments with a second laser. Such experiments are presently hampered by the low power of the F-center laser at the DF monomer frequencies.

Acknowledgment. Support for this research is gratefully acknowledged from the National Science Foundation (Grant No. CHE-93-18936) and the Donors of the Petroleum Research Fund, administered by the American Chemical Society.

References and Notes

(1) Truhlar, D. G. In *Dynamics of Polyatomic van der Waals Complexes;* NATO ASI Series B; Halberstadt, N., Janda, K. C., Eds.; Plenum: New York, 1990 p 159−185.
(2) Copeland, R. A.; Pearson, D. J.; Robinson, J. M.; Crim, F. F. *J. Chem. Phys.* **1982**, *77*, 3974.
(3) Haugen, H. K.; Pence, W. H.; Leone, S. R. *J. Chem. Phys.* **1984**, *80*, 1839.
(4) Vohralik, P. F.; Miller, R. E. *J. Chem. Phys.* **1985**, *83*, 1609.
(5) Dyke, T. R.; Howard, B. J.; Klemperer, W. *J. Chem. Phys.* **1972**, *56*, 2442.
(6) Lafferty, W. J.; Suenram, R. D.; Lovas, F. J. *J. Mol. Spectrosc.* **1987**, *123*, 434.
(7) Gutowsky, H. S.; Chuang, C.; Keen, J. D.; Klots, T. D.; Emilsson, T. *J. Chem. Phys.* **1985**, *83*, 2070.
(8) Howard, B. J.; Dyke, T. R.; Klemperer, W. *J. Chem. Phys.* **1984**, *81*, 5417.
(9) Pine, A. S.; Lafferty, W. J. *J. Chem. Phys.* **1983**, *78*, 2154.
(10) Pine, A. S.; Lafferty, W. J.; Howard, B. J. *J. Chem. Phys.* **1984**, *81*, 2939.
(11) DeLeon, R. L.; Muenter, J. S. *J. Chem. Phys.* **1984**, *80*, 6092.
(12) Lisy, J. M.; Tramer, A.; Vernon, M. F.; Lee, Y. T. *J. Chem. Phys.* **1981**, *75*, 4733.
(13) Chang, H.-C.; Klemperer, W. *J. Chem. Phys.* **1993**, *98*, 9266; **1994**, *100*, 1; **1996**, *104*, 7830.
(14) Suhm, M. A.; Farrell, J. T., Jr.; McIlroy, A.; Nesbitt, D. J. *J. Chem. Phys.* **1992**, *97*, 5341.
(15) Anderson, D. T.; Davis, S.; Nesbitt, D. J. *J. Chem. Phys.* **1996**, *105*, 4488.
(16) Puttkamer, K. v.; Quack, M.; Suhm, M. A. *Mol. Phys.* **1988**, *65*, 1025.
(17) Puttkamer, K. v.; Quack, M. *Chem. Phys.* **1989**, *139*, 31.
(18) Puttkamer, K. v.; Quack, M. *Mol. Phys.* **1987**, *62*, 1047.
(19) Quack, M.; Suhm, M. A. *Chem. Phys. Lett.* **1990**, *171*, 517.
(20) Quack, M.; Suhm, M. A. *J. Chem. Phys.* **1991**, *95*, 28.
(21) Jensen, P.; Bunker, P. R.; Karpfen, A.; Kofranek, M.; Lischka, H. *J. Chem. Phys.* **1990**, *93*, 6266.
(22) Bunker, P. R.; Kofranek, M.; Lischka, H.; Karpfen, A. *J. Chem. Phys.* **1988**, *89*, 3002.
(23) Alexander, M. H.; DePristo, A. E. *J. Chem. Phys.* **1976**, *65*, 5009.
(24) Lischka, H. *Chem. Phys. Lett.* **1979**, *66*, 108.
(25) Epa, V. C.; Bunker, P. R. *J. Mol. Spectrosc.* **1991**, *150*, 511.
(26) Hancock, G. C.; Truhlar, D. G.; Dykstra, C. E. *J. Chem. Phys.* **1988**, *88*, 1786.
(27) Sun, H.; Watts, R. O. *J. Chem. Phys.* **1990**, *92*, 603.

(28) Marshall, M. D.; Jensen, P.; Bunker, P. R. *Chem. Phys. Lett.* **1991**, *176*, 255.
(29) Bunker, P. R.; Jensen, P.; Karpfen, A.; Kofranek, M.; Lischka, H. *J. Chem. Phys.* **1990**, *92*, 7432.
(30) Zhang, D. H.; Wu, Q.; Zhang, J. Z. H.; von Dirke, M.; Bačić, Z. *J. Chem. Phys.* **1995**, *102*, 2315.
(31) Zhang, D. H.; Wu, Q.; Zhang, J. Z. H. *J. Chem. Phys.* **1995**, *102*, 124.
(32) Kofranek, M.; Lischka, H.; Karpfen, A. *Chem. Phys.* **1988**, *121*, 137.
(33) Barton, A. E.; Howard, B. J. *Faraday Discuss. Chem. Soc.* **1982**, *73*, 45.
(34) Zhang, D. H.; Zhang, J. Z. H. *J. Chem. Phys.* **1993**, *99*, 6624.
(35) Huang, Z. S.; Jucks, K. W.; Miller, R. E. *J. Chem. Phys.* **1986**, *85*, 3338.
(36) Pine, A. S.; Fraser, G. T. *J. Chem. Phys.* **1988**, *89*, 6636.
(37) Halberstadt, N.; Brechignac, Ph.; Beswick, J. A.; Shapiro, M. *J. Chem. Phys.* **1986**, *84*, 170.
(38) Dayton, D. C.; Jucks, K. W.; Miller, R. E. *J. Chem. Phys.* **1989**, *90*, 2631.
(39) Bohac, E. J.; Marshall, M. D.; Miller, R. E. *J. Chem. Phys.* **1992**, *96*, 6681.
(40) Marshall, M. D.; Bohac, E. J.; Miller, R. E. *J. Chem. Phys.* **1992**, *97*, 3307.
(41) Bohac, E. J.; Miller, R. E. *J. Chem. Phys.* **1993**, *99*, 1537.
(42) Bemish, R. J.; Wu, M.; Miller, R. E. *Faraday Discuss. Chem. Soc.* **1994**, *97*, 57.
(43) Pine, A. S.; Howard, B. J. *J. Chem. Phys.* **1986**, *84*, 590.
(44) Farrell, J. T., Jr.; Suhm, M. A.; Nesbitt, D. J. *J. Chem. Phys.* **1996**, *104*, 9313.
(45) Fraser, G. T.; Pine, A. S. *J. Chem. Phys.* **1989**, *91*, 633.
(46) Nesbitt, D. J.; Field, R. W. *J. Phys. Chem.* **1996**, *100*, 12735, and references cited therein.
(47) Oudejans, L.; Miller, R. E. *J. Phys. Chem.* **1995**, *99*, 13670.
(48) Loesch, H. J.; Remscheid, A. *J. Chem. Phys.* **1990**, *93*, 4779.
(49) Rost, J. M.; Griffin, J. C.; Friedrich, B.; Herschbach, D. R. *Phys. Rev. Lett.* **1992**, *68*, 1299.
(50) Wu, M.; Bemish, R. J.; Miller, R. E. *J. Chem. Phys.* **1994**, *101*, 9447.
(51) Klopper, W.; Quack, M.; Suhm, M. A. *Chem. Phys. Lett.* **1996**, *261*, 35.
(52) Bohac, E. J.; Miller, R. E. *Phys. Rev. Lett.* **1993**, *71*, 54.
(53) Oudejans, L.; Miller, R. E. To be published.
(54) Bemish, R. J.; Bohac, E. J.; Wu, M.; Miller, R. E. *J. Chem. Phys.* **1994**, *101*, 9457.
(55) Oudejans, L.; Miller, R. E.; Hase, W. L. *Faraday Discuss. Chem. Soc.* **1995**, *102*, 323.
(56) Light, J. C. *Faraday Discuss. Chem. Soc.* **1967**, *44*, 14.
(57) Zhang, D. H.; Zhang, J. Z. H. *J. Chem. Phys.* **1993**, *98*, 5978.